


# Chromia Scale Thermally Grown on Pure Chromium Under Controlled $p(\text{O}_2)$ Atmosphere: II—Spallation Investigation Using Photoelectrochemical Techniques at a Microscale

L. Latu-Romain<sup>1</sup> · Y. Parsa<sup>1</sup> · S. Mathieu<sup>2</sup> · M. Vilasi<sup>2</sup> · Y. Wouters<sup>1</sup> 

Received: 24 November 2017 / Revised: 12 March 2018 / Published online: 10 April 2018  
© Springer Science+Business Media, LLC, part of Springer Nature 2018

**Abstract** Pure chromium oxidized at 900 °C at low oxygen partial pressure ( $10^{-12}$  atm) gives duplex  $\text{Cr}_2\text{O}_3$  scale with an internal part made of equiaxed grains and exhibiting an n-type conduction, and an external part made of columnar grains and exhibiting a p-type conduction. Spalled regions occurring during cooling have been studied with photoelectrochemical techniques at a microscale. New information in the form of a specific image (structural quality image) could be obtained and revealed a level of structural defect density in the internal chromia subscale higher than that measured in the non-spalled region. The results complement the spallation scenario proposed in part I of this work.

**Keywords** Chromia · Photoelectrochemistry · Spallation

## Introduction

It was shown in part I of this work that spallation observed on duplex n-type and p-type chromia scales isothermally grown on pure chromium at 900 °C and a  $p(\text{O}_2)$  of  $10^{-12}$  atm during 30 min occurs during sample cooling. The debonding of the scale takes place at the metal/oxide interface, and the uncovered metal can be then reoxidized at lower temperature. Here, a spalled region is studied by photoelectrochemistry at the microscale. MicroPEC and in particular this setup has proven to be successful in the past to characterize oxide scales. For example, microPEC has allowed to accurately study intermetallics oxidation in thin zirconia scales thermally

---

✉ Y. Wouters  
yves.wouters@univ-grenoble-alpes.fr

<sup>1</sup> CNRS, SIMaP, Université Grenoble Alpes, 38000 Grenoble, France

<sup>2</sup> IJL, Université de Lorraine, 54011 Nancy, France

grown on Zircaloy-4. Lateral distribution of iron and chromium oxides, signed by their respective gap, was imaged in the  $\text{ZrO}_2$  scale with a microscopic resolution [1, 2]. The technique was also used to characterize the nature of different oxides forming the multilayer structure resulting from the exposition of nickel-base alloys intended for pressurized water reactor in primary simulated medium [3]. More recently, photocurrent images could be recorded on ferritic and austenitic grains of a 2205 duplex stainless steel sample thermally grown under water vapor/nitrogen mixtures [4].

## Experimental Procedures

This localized photoelectrochemical (noted as PEC) technique used in this work is so-called microPEC in the rest of this paper. The setup presented in Fig. 1 was developed in our laboratory and is controlled by a homemade software. An argon laser (Innova 90C-A6 from Coherent) was used as the light source. The light was chopped at the frequency  $f = 63$  Hz via an optic modulator, injected in an inverted microscope (IX71 from Olympus) and focused in a long working distance objective ( $\times 50$ ) specially designed for UV (LCD Plan Apo NUV 50 from Mitutoyo). The calculations show that the resolution, essentially conditioned by the numerical aperture of the objective, is of the order of  $\lambda$ , i.e., approximately 350 nm at  $\lambda = 351.1$  nm ( $E = 3.53$  eV). The light power  $P$  can be controlled from the laser

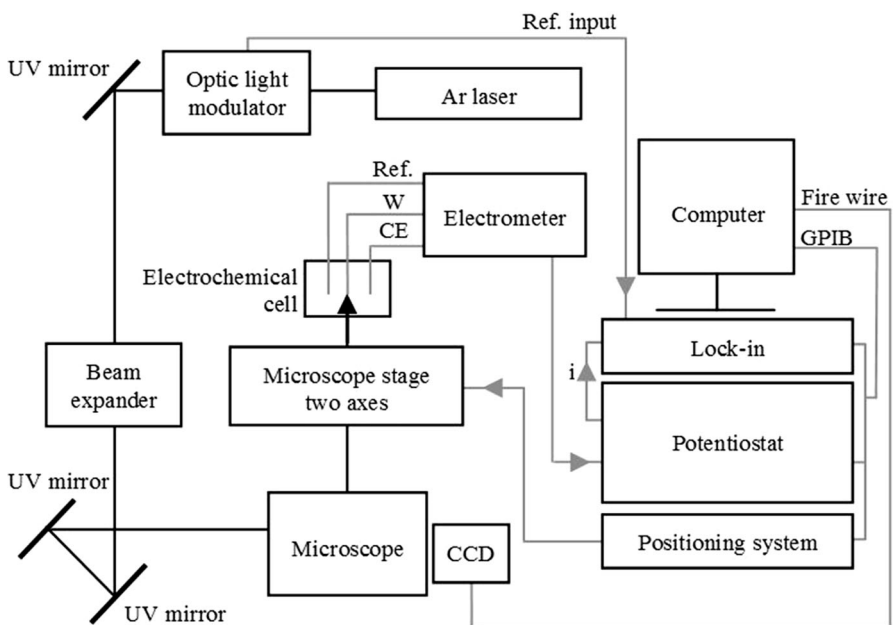


**Fig. 1** Schematic representation of the laboratory-made microPEC

device itself but also by using different filters positioned at the microscope input. The photon flux  $\Phi$  can be expressed as:

$$\Phi = P\lambda(hc)^{-1} \quad (1)$$

where  $h$  is the Planck's constant and  $c$  the speed of light. At  $\lambda = 351.1$  nm and  $P \sim 100$  mW, the calculated photon flux  $\Phi$  is in the range of  $10^{17}$  photons  $s^{-1}$ .

Images were recorded by moving the sample with respect to the laser beam using a high-resolution two-axis motorized stage microscope stage (Scan IM1206100 from Marzhauser, minimum step size: 100 nm). The applied potential was controlled by a potentiostat (273A from Princeton Applied Research), and a lock-in technique was applied to separate the photocurrent from the total electrochemical current. For that purpose, the current output of the potentiostat was connected to the signal input of the lock-in amplifier (Stanford Research SR830) and the trigger signal of the optic light modulator was fed to the reference input of the lock-in amplifier. In parallel, the dephasing angle was also measured and the optical image of the sample was recorded by a CCD camera. Typically, a whole set of 20 images (10 for photocurrent and 10 for dephasing angle) could be obtained after approximately 60 h. Each image included 90,000 points ( $300 \times 300$ ), that is to say, close to 2 millions of points ( $\sim 125$  ms was required by point). The laser was able to provide different monochromatic lines in the visible and UV as described in Table 1. According to the bandgaps measured on chromia scales in part I of this work ( $\sim 3$  and  $\sim 3.6$  eV), the use of UV lines is needed to measure photocurrent, but due to opacification of the laser front mirror, the power of lines in UV decreases with time. In particular, after a few hundred of working hours, the line in deep UV ( $\lambda = 334.4$ ,  $E = 3.71$  eV) is no longer available. Consequently, microPEC experiments have been performed with the wavelength of 351.1 nm ( $E = 3.53$  eV). It was expected, this way, to be able to analyze at least the low-energy contribution of bandgap  $E_g \sim 3$  eV (internal n-type chromia subscale).

## Results and Discussion

Figure 2 presents microPEC analysis of the spalled region presented in part I of this work. A series of photocurrent images  $600 \times 600$   $\mu\text{m}$  (point spacing: 2  $\mu\text{m}$ ) have been recorded at the energy  $E = 3.53$  eV and at several applied potentials ( $V$ ) varying from  $-500$  to  $-50$  mV/MSE—with a 50 mV step. The spalled zone is clearly imaged and exhibits, whatever the applied potential, an average photocurrent value higher than the one observed in the non-spalled zone. All around the spalled zone, the level of photocurrent is much lower than in the rest of the image. This observation should be compared with SEM top-view observation presented in part I of this work showing that the oxide scale around the spalled zone appears debonded in a few micrometer bands in length. Areas of disbondment can stop the diffusion of electronic carriers through the oxide scale and explain the decrease in the photocurrent. It must be also underlined that whatever the coordinates ( $x$ ,  $y$ ) on these images, the photocurrent  $I_{ph}$  increases when the applied

**Table 1** Main lines available with the argon laser

Wavelength $\lambda$ (nm)	Visible										UV	
	514	501.7	496.5	488	476.5	472.5	465.8	457.9	454.5	363.8	351.1	334.4
Energy $E$ (eV)	2.41	2.47	2.50	2.54	2.60	2.62	2.66	2.71	2.73	3.41	3.53	3.71
Power (mW)	1000	~ 70	~ 90	900	250	700	< 10	100	< 10	60	150	< 30

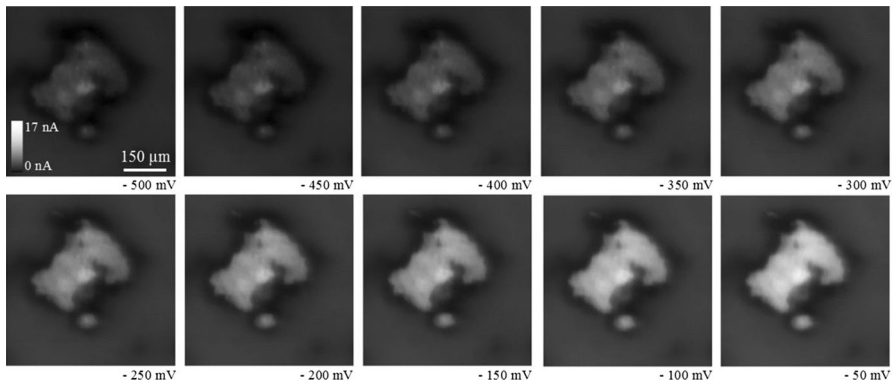


**Fig. 2** MicroPEC analysis of the spalled region. Photocurrent images  $600 \times 600 \mu\text{m}$  (point spacing:  $2 \mu\text{m}$ ), obtained on pure Cr oxidized at  $900 \text{ }^\circ\text{C}$  during 30 min at a  $p(\text{O}_2)$  of  $\sim 10^{-12}$  atm,  $E = 3.53 \text{ eV}$ , recorded at several applied potentials ( $V$ ) varying from  $-500$  to  $-50 \text{ mV/MSE}$ —with a  $50 \text{ mV}$  step

potential  $V$  increases. Consequently, only n-type chromia is recorded on these images.

Concerning the spalled zone itself, this observation is consistent with the results obtained in the part I of this work, i.e., the regrowth of an n-type chromia. Concerning the non-spalled zone, a duplex structure with an internal n-type chromia and an external p-type chromia had been detected in part I, but the external subscale is not detected in the present images. This observation can be explained if we assume that the energy of the incident light ( $E = 3.53 \text{ eV}$ ) is probably not high enough to photogenerate electron hole pairs in the p-type chromia (bandgap  $E_g \sim 3.6 \text{ eV}$ ). Nevertheless, the presence of the external subscale is revealed in Fig. 3 with on the left (a) the photocurrent image ( $E = 3.53 \text{ eV}$ ,  $V = 0 \text{ mV}$ ) and on the right (b) the dephasing angle image recorded at the same conditions. Indeed, the

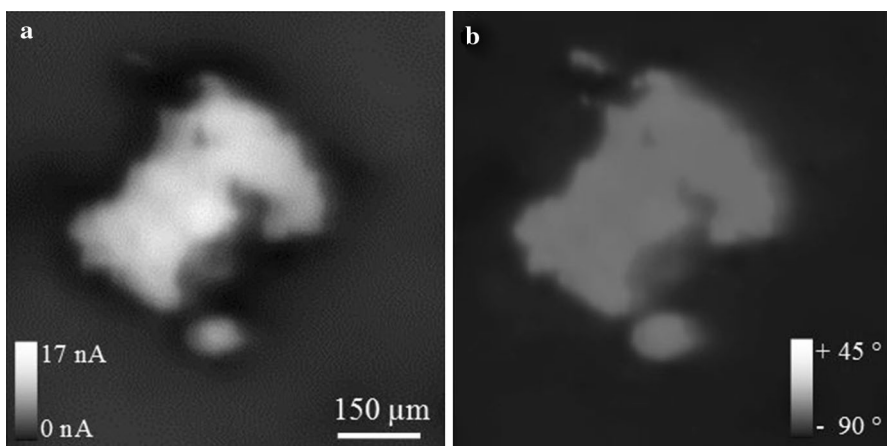


**Fig. 3** Pure Cr oxidized at  $900 \text{ }^\circ\text{C}$  during 30 min at a  $p(\text{O}_2)$  of  $\sim 10^{-12}$  atm, images  $600 \times 600 \mu\text{m}$  (point spacing:  $2 \mu\text{m}$ )  $E = 3.53 \text{ eV}$ ,  $V = 0 \text{ mV/MSE}$ . **a** Photocurrent image, **b** dephasing angle image

evolution of the dephasing angle from spalled zone to non-spalled zone (shift from  $-80^\circ$  to  $30^\circ$ ) corresponds to the beginning of the inversion of the photocurrent sign and reveals indirectly the presence of the external subscale.

In order to go further, a more advanced analysis of those data is needed. For that, photocurrent must be first described.

The parameters involved in photoelectrochemical measurements are numerous and are not all controlled. The development of a model describing the phenomena in a complete way thus proves to be very delicate. A first model describing the behavior of an ideal semiconductor, that is to say without taking into account the recombination phenomena, and its interface with an electrolyte under illumination was proposed in 1959 by Gärtner and improved in 1977 by Butler [5, 6]. This model leads to the following expression of the photocurrent:

$$I_{\text{ph}} = q\Phi_0 \left\{ 1 - (e^{-\alpha_\lambda W_{\text{sc}}}) (1 + \alpha_\lambda L_p)^{-1} \right\} \quad (2)$$

where  $q$  is the elementary charge of the electron,  $\Phi_0$  the incident photons flux,  $\alpha_\lambda$  the absorption coefficient of the oxide at the wavelength  $\lambda$ ,  $L_p$  the diffusion length of the minority electronic carriers and  $W_{\text{sc}}$  the depth of the space charge region which can be expressed as:

$$W_{\text{sc}} = \sqrt{\frac{2\varepsilon\varepsilon_0}{qN_d}} \sqrt{V - V_{\text{fb}}} \quad (3)$$

where  $\varepsilon$  is the dielectric permittivity of the oxide,  $\varepsilon_0$  the vacuum permittivity,  $N_d$  the concentration of the major carriers,  $V$  the applied potential and  $V_{\text{fb}}$  the flat band potential of the oxide.

The absorption coefficient is expressed as:

$$\alpha_\lambda = A(h\nu - E_g)^n (h\nu)^{-1} = \delta_p^{-1} \quad (4)$$

where  $A$  is a constant,  $h$  the Planck's constant,  $\nu$  the light frequency,  $E_g$  the bandgap,  $n$  equal to 1/2 (direct transition) or 2 (indirect transition) and  $\delta_p$  the penetration depth of light.

In conventional cases, the penetration depth of light  $\delta_p$  is greater than  $W_{\text{sc}}$ . All the photogenerated species are therefore not subjected to the action of the electric field, but they may contribute to the photocurrent if their diffusion length  $L_p$  is high enough to generate their flow in the space charge zone and Eq. 2 can be linearized:

$$I_{\text{ph}} = q\Phi_0 A (h\nu - E_g)^n (h\nu)^{-1} \sqrt{\frac{2\varepsilon\varepsilon_0}{qN_d}} \sqrt{V - V_{\text{fb}}} \quad (5)$$

At this point of the discussion, the modeling concerns an ideal semiconductor and does not take into account the recombination phenomenon of electron hole pairs. In particular, many potential experimental spectra cannot be accounted for on the basis of Eq. 5, if particular those of concave shape. We propose to improve this model by the introduction of a new parameter taking into account the level of recombination

center in the oxide scale. Figure 4 presents a schematic representation of the recombination of an electron diffusing in the conduction band (case of an n-type semiconductor). When the level of recombination center increases, the photocurrent decreases.

Recombination centers are generated due to the development of stress in the oxide scale during the oxidation. At every time, part of this stress is relaxed, in particular with creep relaxation [7], but another part is converted into structural defects as dislocations, microporosities, microseparation located either in the volume of grains or at the grain boundaries, or at the metal/oxide interface. Figure 5 illustrates such structural defects. As a consequence, PEC can indirectly detect the recombination centers. Indeed, structural defects can impact the shape of the potential spectrum as illustrated in Fig. 6a [8]. In the case of a quasi-perfect semiconductor, that is to say without any structural defect, the photocurrent increases to its maximum very rapidly. In contrast, when the density of recombination centers (noted as  $\omega_r$ ) increases, the photocurrent  $I_{ph}$  increases less rapidly. In others words,  $\omega_r$  decreases when the area of this spectrum (i.e., the mathematical integral  $\int I_{ph} dV$ ) increases. Nevertheless, the exact evolution is not known and that reasoning stays at this step qualitative (see Fig. 6b).

Previous works have already validated this approach, in particular in the case of the thermal oxidation of pure titanium in oxygen or water vapor [9–12]. When exposed to pure oxygen for a few hours, oxide scales thermally grown on pure titanium at 850 °C develop periodic microcracks localized at the metal/oxide interface due to the accumulation of growth stresses. Microdecohesion and level of structural defects were clearly imaged with PEC techniques.

In order to visualize these fluctuations, we propose to build a new image giving the evolution of  $\int I_{ph} dV$ . To achieve this, from the series of photocurrent images presented in Fig. 2, the local potential spectrum was extracted at every coordinate ( $x, y$ ), and from each spectrum, the value of  $\int I_{ph} dV$  was calculated. After normalization on the parameters applied potential and photocurrent, this value could be finally plotted on a new image so-called structural quality image (SQI). SQI and photocurrent images are presented in Fig. 7a, b. Once again, the spalled zone is clearly imaged on SQI but with a particular effect: the spalled zone is bordered by a

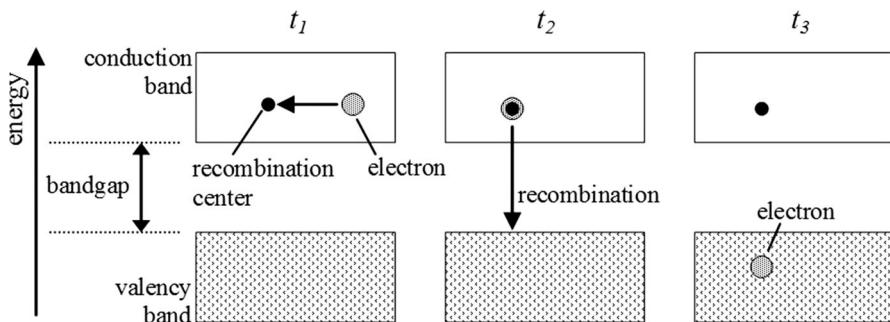


**Fig. 4** Schematic representation of the recombination of an electron diffusing in the conduction band (case of an n-type semiconductor)

**Fig. 5** Schematic representation of the possible nature of a recombination center in an oxide scale

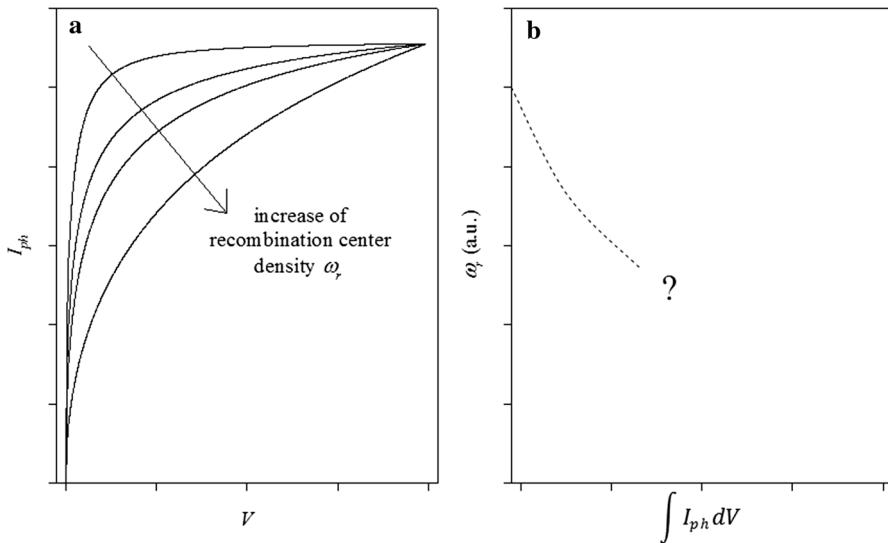
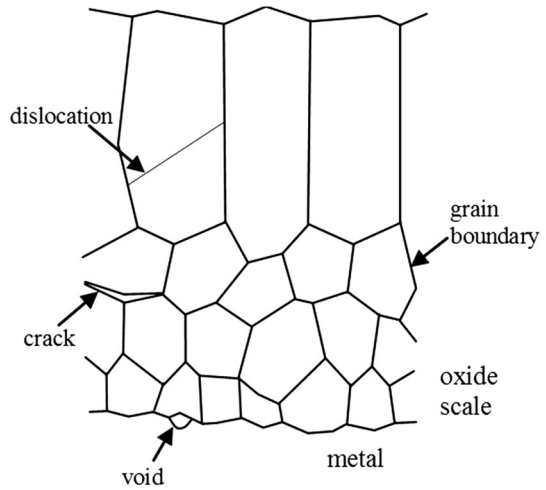


**Fig. 6** **a** Evolution of potential spectra shape with the recombination center density  $\omega_r$ , **b** hypothesized evolution of  $\omega_r$  versus  $\int I_{ph} dV$

dark (resp. light) zone on its left-bottom (resp. top-right) part. At this point, this observation is not well understood.

However, in Fig. 8 the correlation analysis between images 7a, b shows interesting result. To build this image, at each coordinate  $(x, y)$ ,  $I_{ph}$  modulus was extracted from photocurrent image and was plotted as a function of SQI. The density of experimental points in the  $I_{ph} - SQI$  graph was mapped to a color scale. Two groups of points can be observed. The first one with high photocurrent and low



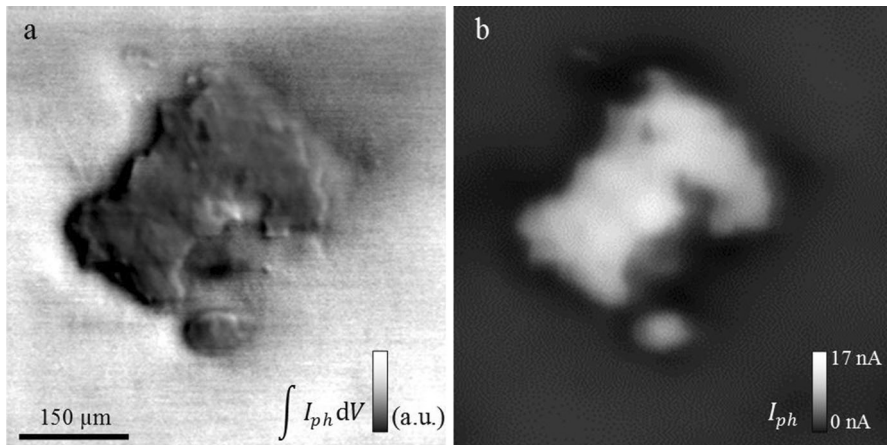


**Fig. 7** Chromia scale thermally grown at 900 °C and a  $p(\text{O}_2) \sim 10^{-12}$  atm during 30 min, **a** structural quality image SQI, **b** photocurrent image ( $E = 3.53$  eV,  $V = 0$  mV/MSE)

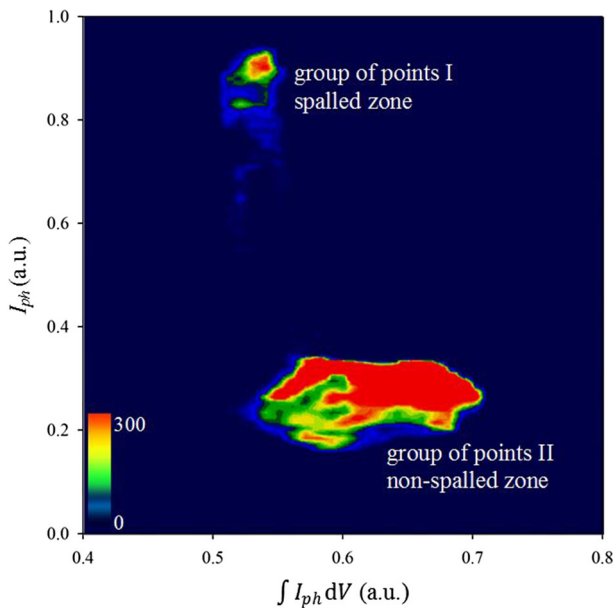


**Fig. 8** Correlation analysis between photocurrent image (7b) and SQI (7a). The photocurrent has been normalized between 0 and 1

SQI corresponds to the spalled zone. In contrast, the second one with low photocurrent and higher SQI corresponds to the non-spalled zone.

At this point of the discussion, several facts need to be recalled:

- a single n-type chromia was observed in the spalled zone (result obtained in part I of this work),

- a duplex structure with an external p-type chromia and an internal n-type chromia was observed in the non-spalled zone (result obtained in part I of this work),
- due to the laser light energy ( $E = 3.53$  eV),  $I_{ph}$  image and SQI only detect n-type chromia ( $E_g \sim 3$  eV),
- the higher the SQI is, the lower the recombination center density is.

From that, results can be interpreted as follows and are summarized in Fig. 9. Concerning the non-spalled zone, the low photocurrent signal can be explained if we assume that part of the light is absorbed by the external subscale. More interestingly, it can be concluded that two sorts of internal n-type chromia have been studied with SQI:

- the first one observed in non-spalled zone is 30 min old ( $\sim 500$  nm in thickness, see Fig. 3b of part I of this work) and exhibits a low level of recombination center (high SQI).
- the second one observed in spalled zone is assumed to correspond to the reoxidation of the uncovered metal after spallation of the scale during the cooling. As a consequence, this layer is probably a few seconds old ( $< 100$  nm in thickness, see Fig. 3c of part I of this work) and exhibits a high level of recombination center (low SQI).

In order to interpret these observations, we propose to refer back to what was concluded in the part I of this work. The inward growth of the internal subscale (n-type chromia) may generate compressive stress in the oxide closed to the internal interface. Part of the stress can be continuously converted into microstructural defects (i.e., recombination centers) in the scale during the thermal oxidation. Over time, part of these defects can be itself continuously restored at high temperature,

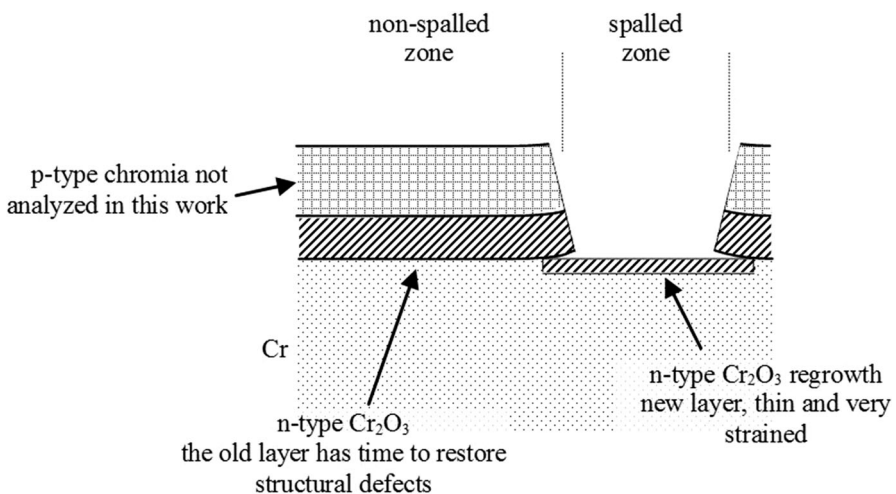


**Fig. 9** Schematic view of the spallation

probably in the whole scale. Consequently, a competition occurs between these two processes: generation and restoration of microstructural defects. Concerning a few seconds layer old, it is assumed that the competition can turn in favor of a high level of recombination center. To the contrary, for an older scale, the level of recombination center can appear lower.

Several spalled regions from different samples obtained with identical experimental conditions have been studied with PEC techniques and exhibit the same characteristics that ones presented in this article.

## Conclusions

Results obtained with PEC technique at a microscale complements and reinforces the spallation scenario presented in part I of this work: the scale decohesion takes place at the metal/oxide interface during the cooling. A microscopic view of generation and restoration of structural defects in chromia scales was produced by constructing of a specific photoelectrochemical image. This work (part I and part II) has shown an original behavior of chromia scales grown on pure chromium at very low oxygen partial pressures. It is intended to continue the study with PEC techniques at higher  $p(\text{O}_2)$ . Studies carried out by PEC techniques, used at different scales, provide interesting results that will require in the future to be coupled with other techniques able to bring additional information, in particular concerning residual stress measurements with Raman spectroscopy and microstructure observations with TEM ASTAR.

**Acknowledgements** This work has benefited from the support of the PSEUDO project of the French National Research Agency (ANR) and was performed within the framework of the Centre of Excellence of Multifunctional Architected Materials “CEMAM” n°AN-10-LABX-44-01 funded by the “Investments for the Future” Program. Special acknowledgments are given to Gilles Renou for his precious help on TEM microscope.

## References

1. F. Atmani, Y. Wouters, A. Galerie and J.-P. Petit, *Materials Science Forum* **595–598**, 571 (2008).
2. Y. Wouters, A. Galerie and J.-P. Petit, *Materials at High Temperatures* **26**, 9 (2009).
3. L. Marchetti, S. Perrin, Y. Wouters, F. Martin and M. Pijolat, *Electrochimica Acta* **55**, 5384 (2010).
4. A. Srisrual, J.-P. Petit, Y. Wouters, C. Pascal and A. Galerie, *Materials at High Temperatures* **28**, 349 (2011).
5. W. W. Gärtner, *Physical Review* **116**, 84 (1959).
6. M. A. Butler, *Journal of Applied Physics* **48**, 1914 (1977).
7. H. E. Evans and M. P. Taylor, *Surface and Coatings Technology* **94–95**, 27 (1997).
8. Y. Marfaing in *Interface Semi-Conducteur/Electrolyte* (Ecole CNRS Aussois, 1984), pp. 35–47.
9. Y. Wouters, A. Galerie, P. Bouvier, M. Mermoux and J.-P. Petit, *Materials at High Temperatures* **22**, 315 (2005).
10. Y. Wouters, L. Marchetti, A. Galerie and J.-P. Petit, *Corrosion Science* **50**, 1122 (2008).
11. Y. Wouters, J.-P. Petit and A. Galerie, *Solid State Ionics* **104**, 89 (1997).
12. A. Galerie, Y. Wouters and J.-P. Petit, *Materials Science Forum* **251–254**, 113 (1997).